

An electrical study of single-ended analog interconnect cables

Milind N. Kunchur

University of South Carolina, Columbia, South Carolina, U.S.A.

Abstract: *The influence of interconnecting cables on an audio system’s performance is a controversial issue. This is partly because commonly measured parameters such as resistance, reactance, frequency response, and common distortions do not show meaningful differences. The present electrical study of line-level single-ended (unbalanced) analog interconnects, provides a more comprehensive picture surpassing the common specifications. It was found that uncommon time-domain effects such as reflection sequences and non-ideal capacitive behavior, along with noise, can better distinguish the electrical performance of interconnects of different grades.*

I. Introduction

Music reproduction spans a wide spectrum in sonic fidelity, ranging from mainstream consumer applications (e.g., portable devices and computer audio) to elaborate “high-end audio” (HEA) systems. The latter typically consist of separate specialized components such as optical transports, digital-to-analog converters, preamplifiers, power amplifiers, and loudspeakers. Interlinking cables between these components are an inevitable necessity. The possibility that cables might affect a system’s sonic performance remains a controversial and contentious subject, because of the rarity of published research proving audibility of cables (and for that matter the audibility of any audio-configuration change other than replacing the loudspeakers). Nevertheless, there is a sea of anecdotal claims by audiophiles that cables influence sonic performance, and there exists a well-established audio-cable industry.

Skeptics dismiss cable audibility as a “snake-oil claim” partly on the grounds that certain measurements—for example, of RLC (resistance, inductance, and capacitance) and FR (frequency response)—do not reveal meaningful differences between cables. Also cables are viewed as non-distorting linear networks between components that can be characterized by fixed transfer functions. However, as shown here, such views of how cables operate are incomplete and incorrect.

Recently published work [1] proved psychoacoustic discernment of two analog cable pathways, demonstrating audibility of the smallest change in an audio chain up to that point. The work underscored the need to use an audio system of sufficient fidelity to avoid masking subtle differences, and emphasized the benefit of extended-duration listening that resembles audiophile auditioning. Those experiments compared a balanced-cable pathway with a single-ended (unbalanced) pathway, because this could be done without adding external switch boxes and wiring. However, that approach prevented distinguishing whether noise differences between pathways originated from the balanced-versus-unbalanced topology or the cables themselves. It also prevented studying TD (time-domain) effects, as this would have required (for the balanced cable) additional circuitry (differential amplifiers, etc.) which would have introduced its own signal alterations. Various previous works have emphasized the importance of TD signal alterations at higher fidelity [2–12].

To address some of these issues and conduct an investigation that includes TD electrical behaviors, the present work compared single-ended interconnects and probed uncommon TD effects such as non-ideal capacitive decays and reflection sequences. These TD effects have considerably higher magnitudes than variations in FR and the effects of R and L, and are therefore more likely to make a sonic difference. The measurements developed here show a demonstrable progressive improvement with the cable’s “grade” (generic, entry-level, and higher-end ones from commercially available cables) providing some additional objective measures for judging a cable’s electrical accuracy, whether or not it makes a discernable sonic difference in a particular system.

II. Electrical behavior of interconnect cables

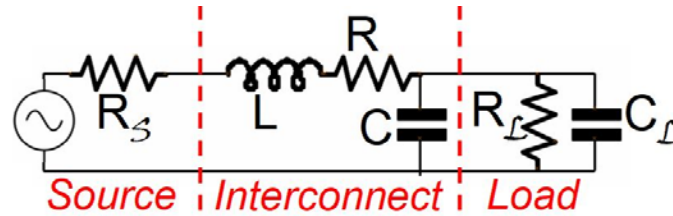


Fig. 1. A typical application circuit hosting an interconnect. Subscripts “ \mathcal{S} ” and “ \mathcal{L} ” refer to source and load respectively.

2.1 Low-frequency equivalent circuit and basic parameters

Fig. 1 shows the typical high-impedance circuit hosting an interconnect (approximated here as a distributed-linear-RLC circuit not incorporating the non-linear/TD effects that are discussed below). Many discussions of cables on audio forums are limited to such a framework which, as demonstrated here, is insufficient for fully characterizing interconnect performance. The typical parameter values are such that $R \ll R_S \ll R_L$ (with $R < 1 \Omega$, $R_S \sim 100\text{--}1000 \Omega$, and $R_L \sim 10 \text{ k}\Omega\text{--}1 \text{ M}\Omega$). The inductive decay time is given by

$$\tau_L = L/(R_L + R_S) \approx L/R_L, \quad (1)$$

capacitive decay time by

$$\tau_C = CR_S R_L / (R_L + R_S) \approx CR_S, \quad (2)$$

self-oscillation period by

$$T_{LC} = 2\pi(LC)^{1/2}, \quad (3)$$

and resistive power loss in dB by

$$P_L = 20 \cdot \log[(R + R_L + R_S)/(R_L + R_S)]. \quad (4)$$

Normally $\tau_L \ll \tau_C$ and $P_L \ll 0.001 \text{ dB}$ (see measured values below), so that inductance and resistance are irrelevant for interconnects^a. This holds even including the skin effect, whereby the current is progressively forced out from the interior with increasing frequency and travels within a skin depth

$$\delta = [\rho/(\pi f \mu)]^{1/2}, \quad (5)$$

where ρ , f , and μ are the resistivity, frequency, and permeability respectively. For copper at $f=1 \text{ MHz}$, $\delta = [\rho/(\pi f \mu)]^{1/2} = 65 \mu\text{m}$ far exceeds the typical surface roughness of $\sim 2 \mu\text{m}$, making the skin effect irrelevant (i.e., $P_L \ll 0.001 \text{ dB}$ continues to hold).

2.2 Transmission and non-ideal characteristics

One contribution to an interconnect’s transient response arises from its transmission-line properties, one of which is its characteristic impedance

$$Z = (L/C)^{1/2} \quad (6)$$

and its variation ΔZ over its length (whose indication was taken as the left-to-right-channel fractional discrepancy). Internal reflections are reduced by making ΔZ small (a measure of quality control). End reflections are reduced by matching Z with R_L , R_S , and the connector impedance. A sequence of back-and-forth reflections can add a decaying oscillatory tail to transient edges, whose persistence worsens for longer cables and slower propagation speeds

$$v = c \cdot (\epsilon_r \mu_r)^{-1/2} \approx c \cdot (\epsilon_r)^{-1/2}, \quad (7)$$

where $c = 3.00 \times 10^8 \text{ m/s}$ is the speed of light in free space, ϵ_r is the relative permittivity (dielectric constant), and μ_r is the relative permeability. For interconnects, $\mu_r = 1$ and the main retardation is due to $\epsilon_r > 1$ (for reference, ϵ_r equals 1 and 1.0005 for vacuum and air respectively).

Eq. 2 ($\tau_C \approx CR_S$) represents an ideal exponential decay when the capacitance has a constant value and releases its charge completely and instantaneously, with the only bottleneck for speed being the external resistance. But the reality is more complicated. Electrostatic forces attract a capacitor’s plates closer causing C

^a This may not be true for the low-impedance circuit of a loudspeaker cable.

to change with voltage V and time [13, 14]; this effect will be referred to as *electromotive capacitance*^b. Also the polarization of the dielectric insulation has its own time scale [15] and cannot keep up with a rapidly changing electric field^c. Both of these non-ideal capacitive (NIC) effects lead to a rise in ϵ_r and C (and decrease in v per Eq. 7) at lower f . The cable then cannot be represented by a fixed transfer function and will have a NIC decay lingering past the nominal ($\tau_c \approx CR_S$) exponential decay^{d,e}. The finite decay times prevent the output voltage V_{out} from tracking the input V_{in} instant-for-instant, and contaminate it with its earlier history through the convolution $V_{out}(t) = \int K(t-t') V_{in}(t') dt'$ over $t' = -\infty$ to t , with a kernel $K(t-t')$ that itself depends on signal amplitude and history.

Thus as a rule of thumb, a larger ϵ_r implies a slower dielectric response and more dispersion (propagation speed variation with frequency) [18]. Hence all things being equal, it is desirable to have $\epsilon_r \approx 1$ and $v \approx c$ (Eq. 7). Thus measuring the relative propagation speed v/c provides an efficacious way to assess the *quality* of a cable's capacitance (constancy with frequency). Some cable designs achieve an effective ϵ_r less than the intrinsic material's value by having the electric field reside partly in air through porous (foam) insulation (e.g., Belden 4855R, RG-59 cable) or by conductor geometry (e.g., Nordost Norse 2 cable). Electromotive capacitance and magnetomotive inductance (see footnote d) are best reduced by making the cable structure as rigid as possible. But this conflicts with the advantages of flexibility and insulation porosity. Such challenges undoubtedly contribute to the difficulty (and expense) in optimizing HEA cable designs.

2.3 Idealized transfer function

If the above esoteric effects are neglected, the simplistic circuit of Fig. 1 (including the cable, R_L and R_S ; with $C_L \ll C$, $R \ll R_L$, and $R \ll R_S$) has a complex FR or transfer function^f for steady audio-frequency pure tones that can be approximated by

$$G = V_{out}/V_{in} = 1/[(R_S+R_L)/R_L + j2\pi fCR_S] \quad (8)$$

where $j = (-1)^{1/2}$. The absolute magnitude $|G|$ and phase shift ϕ (in degrees) are given respectively by

$$|G| = |V_{out}/V_{in}| = [\{ (R_S+R_L)/R_L \}^2 + \{ 2\pi fCR_S \}^2]^{-1/2} \quad (9)$$

$$\phi = - (360/2\pi) \tan^{-1} [2\pi fCR_S R_L / (R_S+R_L)]. \quad (10)$$

As demonstrated below, the detailed response is more complicated than represented by the idealized transfer function.

2.4 Noise vulnerability

Noise pickup in cables through EMI (electromagnetic induction) and RFI (radio-frequency interference) is a well known problem that depends not only on how well a cable is shielded but also on details of the grounding scheme and the impedances of the host circuit. These issues are well covered in [19–22]. Noise was found to be the main distinguishing measurement in [1] (where TD measurements were not carried out for the reasons mentioned earlier related to balancing), where their “cable A” (balanced interconnect) had lower noise and a more detailed sound. The present work shows that a similar unbalanced cable has a comparably low noise level, so the superior noise performance seems to be more related to better shielding than to the topology.

^b This effect in cables has been studied in [14]. Some of their relevant findings/points are: (1) C rises over a period of ~ 2 s when V is increased; (2) the effect does not cancel out in balanced cables, but has lower magnitude due to the halved ground-referenced voltage per leg; (3) they did not directly compare cables in listening tests, but used DSP (digital signal processing) simulations of the effect.

^c The four principal dielectric mechanisms are: electronic, ionic, dipolar, and space-charge based. The latter involve moving more mass and charge through greater distances, leading to a higher but slower responding ϵ_r to changing electric fields.

^d There is an analogous *magnetomotive inductance* effect whereby repulsive magnetic forces between oppositely directed currents lead to a larger L at lower f . This will especially affect cables in low-impedance circuits such as for headphones or loudspeakers [16].

^e Another potential source of audible differences in loudspeaker cables was discussed in [17]: A loudspeaker (being a non-linear load and electric generator itself) creates a distortion voltage across its own terminals; this gets “shorted” to a variable degree by the amplifier's output impedance combined with the cable's inductance and resistance.

^f Note that a cable cannot be represented as a simple overall “impedance” even when RLC behave ideally, because not all elements are in series (some are shunts).

III. Experimental Materials and Methods

3.1 Cables Tested

With the purpose of exploring differences between generic interconnects and audiophile ones, only single-ended (with RCA connectors) shielded coaxial style cables were tested since balanced cables are non-existent in entry-level consumer audio. Also TD measurements are more straightforward for single-ended cables. The interconnects' length was chosen to be 2 m long, since differences are more evident for longer lengths, while at the same time this is not an uncommon length for typical applications. The three cables tested[§], labeled S, M, and G are: (S) a ~\$500 "audiophile-grade" interconnect utilizing porous polytetrafluoroethylene dielectric (sold through specialty high-end audio dealers); (M) a ~\$50 entry level interconnect utilizing polyethylene dielectric (sold at appliance and consumer electronics stores); and (G) a generic interconnect utilizing polyvinyl chloride dielectric (sold at general stores for under \$5 or included with inexpensive consumer electronics). The shields of cables S and G are symmetrically grounded at both ends, while cable M's shield is grounded at only the source end (the recommended signal direction is marked with arrows on the jacket^h).

The measurements below find an electrical performance ranking: S, M, and G in agreement with what one might expect based on the pricing and notional quality indicators such as the dielectric insulation.

3.2 Instrumentation and Measurement Techniques

Seven separate experiments rigorously probed signal alterations in interconnects using electrical measurements far surpassing conventional specifications. Rather than using automated "black box" approaches such as REW (Room Equalization Wizard) that do not show the waveform, or off-the-shelf spectrum analyzers, the present work used more exacting first-principles methods: Instead of computer sound cards, typically limited to a 192 kHz sampling rate (i.e., 96 kHz Nyquist frequency and 5.2 μs sampling period), the present work used vastly faster signal sources (e.g., 4 ns pulses) and digital storage oscilloscopes (DSOs) with up to 10 GHz single-shot and 250 GHz random-interleaved sampling rates. Also the detailed TD and noise information gleaned from these independent measurements cannot be matched by oscilloscope "eye diagrams", which conveniently capture multiple signal aspects in a unified measurement (the eye-diagram technique is more valuable for digital-signal transmission than analog). Experiments 2–6 and experiment 7 used LeCroy WaveRunner 204Xi and LT342 DSOs respectively (no probes were used), and followed schemes similar to Fig. 2 with various signal sources.

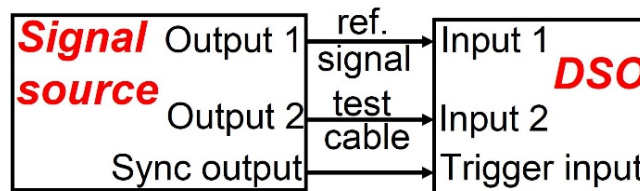


Fig. 2. General setup for frequency-response, time-domain, and noise measurements. ("ref." is "reference".)

The suite of measurements conducted here are tedious and time consuming but yield deeper insights into a cable's electrical behavior. The detailed TD information obtained here cannot be substituted for by the coarse and indirect impulse response derived from an FR, such as measured by an REW based system. The latter's time resolution isn't anywhere near that of the present methods. Also the inversion from FR (even with unlimited frequency resolution and range) to TD works exactly only when non-linear effects are absent.

[§] Interconnect S in this study is similar to interconnect A used in [1], but is single-ended instead of balanced. Interconnect M here is the same as B in [1].

^h Symmetric cables may also have arrows to ensure reinstallation in the same direction after removal to avoid fatiguing the metal by repeated bending and unbending.

IV. EXPERIMENTAL RESULTS

4.1 Experiment 1: Electrical parameters

Table 1: Measured R , L , and C values (averaged for both channels and normalized per meter) and calculated parameters (with $R_S = 100 \Omega$ and $R_L = 10 \text{ k}\Omega$; please see text for formulas) for three interconnect cables. $1 \mu\text{B} = 0.00001 \text{ dB}$. All parameters are proportional to the length except for Z and ΔZ .

Cable	R (m Ω)	L (nH)	C (pF)	Z (Ω)	ΔZ %
S	47.8	95	279	18.5	0.7
M	84.0	638	148	65.7	2.1
G	323	283	239	34.4	14.1
Cable	τ_L (ps)	τ_C (ns)	T_{LC} (ns)	P_L (μB)	
S	9.5	27.9	32.3	4.11	
M	63.8	14.8	61.0	7.27	
G	28.3	23.9	51.7	27.8	

The RLC parameters were measured with an *MCH 2811c* LCR meter using four-terminal Kelvin sensing. C and L were measured at an excitation frequency of $f_E = 10 \text{ kHz}$ with accuracies of $\pm 2 \text{ pF}$ and $\pm 5 \text{ nH}$. R was measured at $f_E = 100 \text{ Hz}$ and 1 kHz , both agreeing within a $\pm 0.05 \text{ m}\Omega$ error. Section II explains the calculated parameters.

From Table 1, one can learn the following:

- (1) While R and P_L do follow the external diameter of the cables and the implied gauges of their conductors, their absolute values are utterly negligible. Thus although the thin generic interconnect's R is 7 times higher than for interconnect S , it would still have to be 11 km long (even including the skin effect, which raises its P_L to 39 μB) to have a 3 dB loss in delivered power!
- (2) Although capacitive effects dominate inductive effects by about a thousand fold, all the nominal reactive times (τ_L , τ_C , and T_{LC}) are very short ($< 100 \text{ ns}$) from a spectral filtering point of view (i.e., $1/2\pi\tau > 2 \text{ MHz}$). As shown below, this fact is mirrored in the frequency response.
- (3) The frequency dependence of C , the main reactive player, was studied in more detail in a separate experiment described below; however, this LCR-meter experiment already shows the following variations of C with f (for $f_E = 100\text{Hz}$, 1 kHz , and 10 kHz): 0.5%, 0.9%, and 8.7% for cables S , M , and G respectively. Thus NIC effects were worse for lower grade interconnects.
- (4) The variability ΔZ —which is related to manufacturing tolerances and controls internal reflections—is tighter for the audiophile grade interconnects (0.7% for S and 2.1% for M) compared to the generic (14.1%). Reflections were studied in a separate experiment described below.

4.2 Experiment 2: Frequency dependence of cable-capacitance

For this experiment, a sinusoidal signal was provided by a Tenma 72-910 Audio Oscillator with an added series resistor to make $R_S = 1 \text{ M}\Omega$. The DSO was set to $R_L = 1 \text{ M}\Omega$ (DC coupling), no BWL (bandwidth limit), and no ERES (enhanced resolution), providing a 500 MHz analog bandwidth. The high R_S configuration (compared to normal operation) allowed a more sensitive study of the cable's capacitance. Note that the measured response is for the Fig. 1 circuit (equations 8–10) not the cable's transfer function, since here V_{in} includes the voltage drop across R_S ; V_{out} is across R_L . In order to better elucidate the capacitive effects, the interconnect lengths were doubled to 4 m by linking the left and right cables in series through an RCA female-to-female coupler.

As plotted in Fig. 3 (a) and (b), there are large changes in the magnitude $|G| = |V_{out}/V_{in}|$ and phase shift ϕ because of the high chosen values of $R_S = R_L = 1 \text{ M}\Omega$. The theoretical curves—representing equations 9 and 10 with C values taken from Table 1—are seen to generally well describe the measured response without adjustable fitting parameters. Deviations from the curves arise from variations in C with f . Equations 9 and 10 can thus be inverted and used as sensitive tools to obtain C as a function of f :

$$C = [(|G|^2 - \{(R_S + R_L)/R_L\}^2)/(2\pi f R_S)^2]^{1/2} \quad (11)$$

$$C = -\tan(2\pi\phi/360) (R_S + R_L)/(2\pi f R_S R_L) \quad (12)$$

Equation 11 (C from measured $|G|$) is sensitive at high f (with $|G|$ becoming flat and useless at low f ; see Fig.

3(a)). Conversely Eq. 12 (C from ϕ) works best at low f (Fig. 3(b)). Fig. 3 (c) shows the composite result. As observed in the previous LCR-meter experiment, C is relatively constant for cables S and M. But for cable G, C varies by 74% (32% over the audible band). Thus a nominal single-frequency measurement (Table 1) gives the wrong impression that all is well with cable G's capacitance.

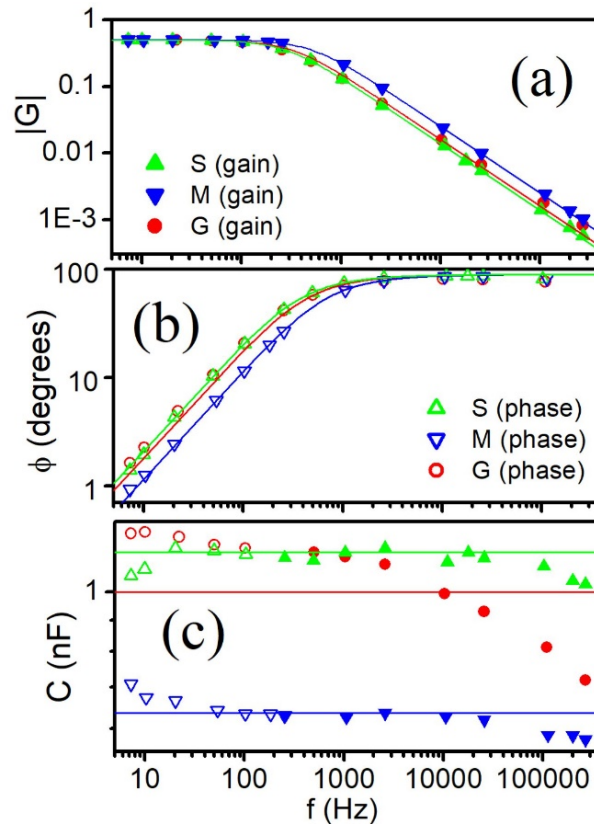


Fig. 3. (a) Measured gain magnitude $|G| = |V_{out}/V_{in}|$ and (b) phase shift ϕ for the circuit in Fig. 1 with $R_S = R_L = 1\text{ M}\Omega$. Solid lines represent equations 9 and 10 without any adjustable fitting parameters. (c) C versus f extracted from above data using equations 11 and 12. Solid lines and curves use LCR-meter measured C values from Table 1 (scaled to 4 m plus 44 pF due to couplers and adaptors).

4.3 Experiment 3: Cable frequency response

Experiment 3 used a similar setup to experiment 2, except for the absence of the series resistor following the source so that $R_S = 600\ \Omega$. The DSO was set to 2 bit ERES and provided a 500 MHz analog bandwidth. An external resistor in parallel with the DSO input rendered a net $R_L = 10\ \text{k}\Omega$, and V_{in} was measured at the cable's input itself. This lower impedance environment better mimics normal interconnect operation and provides the complex frequency response pertinent to audio applications. Single 2m long interconnects were measured.

Fig. 4 shows some example waveforms. The differences are so small that the main curves (V_{in} and V_{out}) practically lie on top of each other and cannot be visually distinguished. But the zoomed view (slanted parallel lines) of the highlighted portion near the origin (after synchronously averaging >10000 sweeps) clearly shows a horizontal time shift Δt . The phase shift can then be found from the amplitudes (A_1 and A_2) and vertical offsets (V_1 and V_2) of the two channels, and Δt , using the equation

$$\phi = 360f \cdot [\Delta t + \{\sin^{-1}(V_2/A_2) - \sin^{-1}(V_1/A_1)\} / \{2\pi f\}]. \quad (13)$$

The gain magnitude is of course

$$|G| = A_2/A_1. \quad (14)$$

This first-principles experimental arrangement can accurately identify extremely minute phase shifts, which might evade black-box approaches like REW and some off-the-shelf spectrum analyzers.

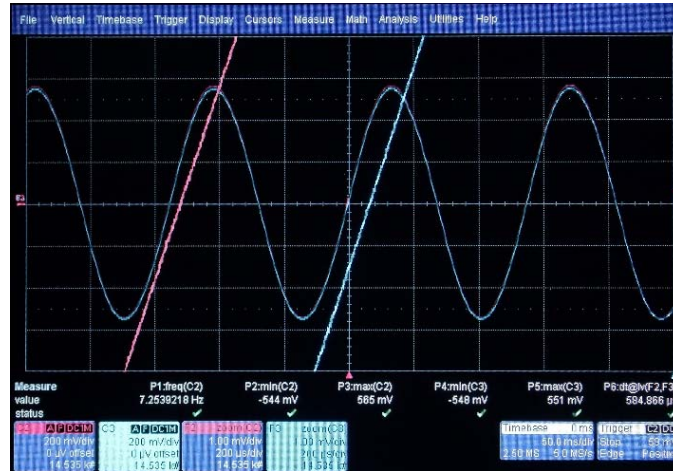


Fig. 4: Oscilloscope screen showing setup for high-precision complex-frequency-response measurements. The main scales are 200 mV/div vertical and 50 ms/div horizontal (with 10 bits vertical and 200 ns horizontal resolution). The slanted lines (a 200X vertical by 250X horizontal zoom near the origin) clearly show the phase difference. The curves represent the average of 14535 individual traces in order to reduce noise.

The values for $|G|$ and ϕ found through this process are plotted in Fig. 5 over a range that surpasses the audible band. $|G|$ is flat within ± 0.03 dB and ϕ varies by less than $\pm 0.06^\circ$, even for the generic interconnect. Such sonically perfect responses feed the skepticism against cable audibility. However, the FR is a just one facet of electrical performance. This work shows that there are other electrical characteristics that differentiate cables that have more potential to distinguish them sonically. On audio forums, interconnect cables are sometimes viewed as frequency-response equalizers. As seen here, this is impossible since the objective FR is essentially flat, at least for the range of interconnects tested here. However, the interconnect may still alter the “subjective FR” (i.e., the timbre or tonal quality of the sound) through the other effects investigated here. As will be discussed in detail elsewhere [23] and noted in [2–10], the onset and offset transients of a note are more influential in determining timbre than the complex FR.

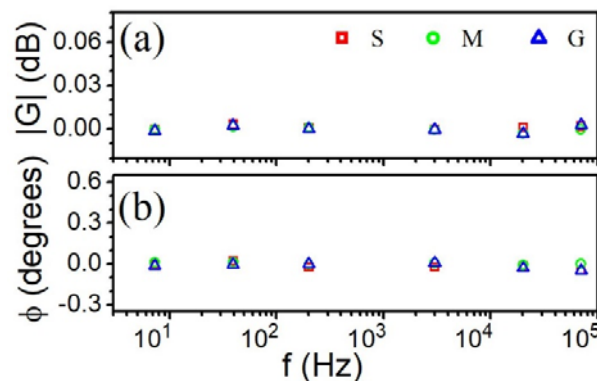


Fig. 5. Complex frequency response of interconnects.

4.4 Experiment 4: Transient response

For experiments 4–6, a Quantum Composers model 9512 dual-channel pulse generator (PG) provided 5V pulses. Their repetition period of 0.025 s contains exactly 1.5 power-line-cycle (PLC) periods of $T_{PLC}=1/60$ s, which dramatically suppresses power line noise (and uncorrelated noise) when an even number of oscilloscope traces are averaged. For this experiment, the DSO triggered on the signal from the test cable itself (i.e., only the middle signal path in Fig. 2 was active). The PG’s output impedance was increased to $R_S = 100 \Omega$ (to simulate a typical HEA component) by adding a 50Ω series resistor, and the interconnect terminated into $R_L = 10 \text{ k}\Omega // C_L = 20 \text{ pF}$ (a typical HEA-component input impedance; the DSO’s input coupling was set to $1 \text{ M}\Omega\text{-DC}$).

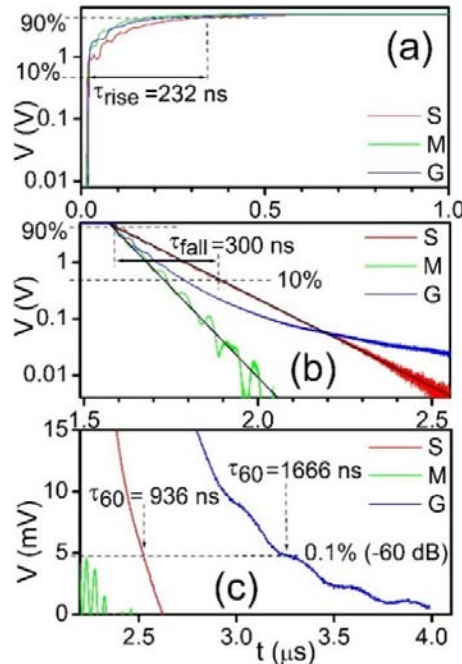


Fig. 6: Transient responses (1000 sweeps averaged) of the three 4m long (doubled) analog interconnect cables (S, M, and G) to square pulses showing the (a) rise, (b) fall, and (c) low-level (mV) tail regions. The solid black lines in (b) represent the exponential functions $V(t) = V_0 \exp[-(t - t_0)/\tau]$ with a plateau voltage of $V_0 = 4.87$ V, time offset of $t_0 = 1.573$ μ s, and exponential decay times of $\tau = 139$ ns and 68 ns for cables S and M respectively. (a) and (b) exemplify (for cable S) the definition of τ_{fall} and τ_{rise} .

Fig. 6 shows the transient responses of the three interconnects to a long (1.572 μ s) square pulse[†]. The nominal (10% to 90%) rise time τ_{rise} is faster than the fall time τ_{fall} for all cables. Interconnect S exhibits an ideal textbook exponential decay $V(t) = V_0 \exp[-(t - t_0)/\tau]$ (see panel (b)). The other audiophile interconnect (M) follows an approximately exponential decay albeit with oscillatory structure superimposed on it. The exponential time constants τ are slightly (~20%) higher than the 4-times length-scaled τ_C values of Table 1 because of stray capacitances of the source, load, adaptors and couplers. The generic cable decays non-exponentially and exhibits an extended decay arising from its NIC behavior; although G's nominal τ_{fall} is shorter than for S (panel (b)) it crosses over to a much longer 60 dB decay time $\tau_{60} = 1.7$ μ s instead of 0.9 μ s (panel (c)).

It is shown below, with full-bandwidth impulse measurements of reflections and measurements of un-averaged noise, that interconnect M has a pronounced lingering RF (radio frequency) tail. This again reinforces how misleading a cable's nominal single-frequency capacitance measurement can be, and the usefulness of fast time-domain measurements for a more complete picture.

4.5 Experiment 5: Signal propagation speed

The basic setup for this experiment is similar to the previous one except that the PG's channel A sent a synchronizing pulse to the external trigger of the DSO, while channel B supplied the narrowest possible pulse (4 ns) after a delay of 6.18 μ s (to surpass trigger related noise) through the test interconnect[‡].

[†] For the high ranges of Fig. 6 (a) and (b), the DSO was run at a 10 GHz single-shot sampling rate and set on 1 V/div scale with no BWL and no ERES. The lower range of Fig. 6 (c) used a 200 mV scale with 200 MHz BWL and 2.5 bits ERES.

[‡] Here again, $R_S = 100$ Ω and $R_L = 10$ k Ω // $C_L = 20$ pF; DSO sampled at a 10 GHz single-shot rate with 1.5 bit ERES and no BWL; and 10000 pulses were synchronously averaged. Absolute amplitudes differ for cables because of different reflection coefficients at the terminations. Effective propagation distance is ~0.07 m greater than the nominal 4 m cable due to the RCA-to-RCA coupler and two BNC-to-RCA adaptors. This plus the oscilloscope's 0.1 ns resolution limit result in an error bar of ± 0.3 ns in time.

The waveforms in Fig. 7 illustrate the absolute propagation times and the inset shows the corresponding speeds. The v/c ranking is as expected from Eq. 7 and the permittivity values of their insulation: $\epsilon_r < 2.1$, $\epsilon_r = 2.2\text{--}2.4$, and $\epsilon_r = 3\text{--}4$ for S, M, and G respectively.

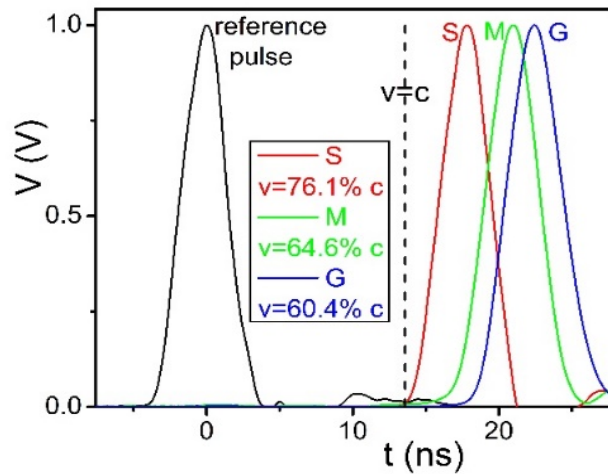


Fig. 7: Normalized pulse-propagation waveforms for 4m long (doubled) interconnects (S, M, and G). The vertical dashed line “ $v=c$ ” indicates the expected arrival time if the distance had been traversed at $c=3 \times 10^8$ m/s, the speed of light in vacuum. The inset box shows the measured propagation speeds as a percentage of c for each interconnect.

4.6 Experiment 6: Reflection sequence

The experimental setup for this is essentially the same as the previous experiment except for a delayed and longer time window (see Fig. 8), to capture the reflection sequence—an RF structure arising from back-and-forth reflections of progressively attenuated amplitudes that persists long after ($t > 100$ ns) the application of the 4 ns pulse. Interconnect G, with the most regular reflection pattern, has a fairly constant period $T_{\text{reflection}} = 23.8 \pm 0.3$ ns that agrees with the total round-trip distance of 4.27m (including adaptors and couplers) divided by the measured propagation speed (see inset of Fig. 7).

This RF tail upon entering subsequent electronics can affect the audio signal like any other input RF noise. However, unlike RF noise picked off the air or circuit noise, the reflection sequence is temporally correlated with the signal, affecting the decay transients of a note. Research on perceptual fusion/segregation of auditory components [24–26] suggests that correlated artifacts ought to have a greater influence on timbre than uncorrelated noise, other factors being equal.

From Table 1, cable M (with $Z = 66 \Omega$) should have a closer match with the 100Ω termination at the source end, than cables G ($Z = 34 \Omega$) and S ($Z = 19 \Omega$). But contrary to expectations cable S has the smoothest decay with least prominent reflections. This suggests that the connectors of cable S may be mitigating reflections, supporting the importance of connectors’ influence in electrical (and potentially sonic) performance.

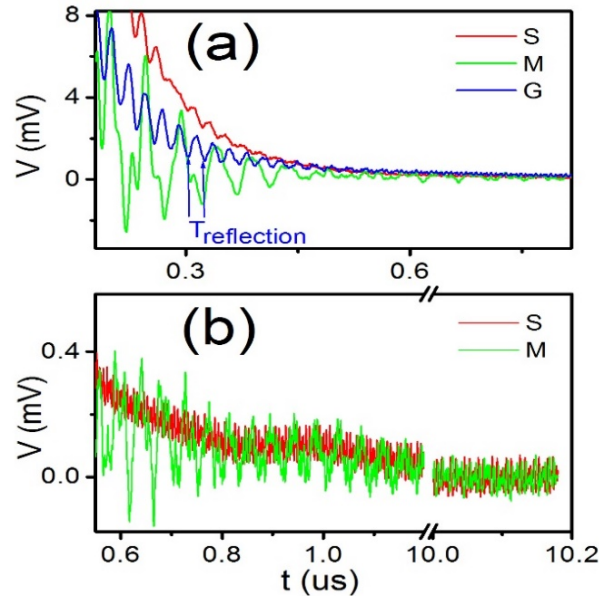


Fig. 8: (a) Impulse response showing sequence of reflections for three 2m long analog interconnect cables (S, M, and G). The period $T_{\text{reflection}}$ agrees with the propagation speed and cable length. (b) Magnified view comparing cables S and M for extended times.

4.7 Experiment 7: Noise

Two types of measurements fully investigated cable noise vulnerability. First, voltage-time waveforms were measured with the left and right members of each interconnect connected to separate channels of the same (switched-off) dual-channel pulse generator, which provided 50 Ω terminations although it did not source a signal. The interconnects' other ends were connected to separate channels of the DSO set to 1 MΩ DC-coupled input and no BWL. All traces were single-shot with random trigger and no averaging. This arrangement allowed noise in both left and right channel cables to be measured simultaneously to study channel correlation. Both the generator and the oscilloscope were grounded at their power outlets, which gave the least overall noise.

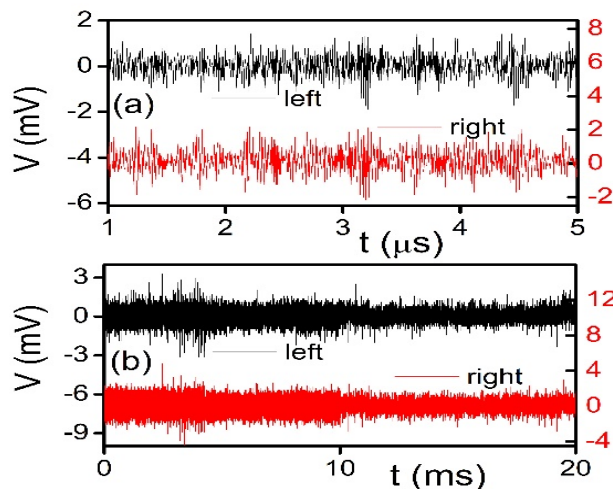


Fig. 9: Noise waveforms in interconnect G show close correlation between left and right channels over two widely separated time scales.

Fig. 9 shows noise waveforms for generic interconnect G. There is a close correlation between the left and right channels, because their separation is much less than RF wavelengths. Such correlated noise will intrusively image in the middle of the reproduced soundstage [27–28] and tend to perceptually interfere with the musical performance. The lesson here is that left and right interconnects should be spaced far apart and not run

close together (which cannot be avoided when the channels are molded together, as in the case of interconnect G).

Next, noise vulnerability was compared for both signal directions (“forward” and “reverse” relative to the marked arrows, if any). The two symmetrically grounded interconnects S and G did not show a directional difference. But the asymmetrically grounded interconnect M showed a striking directional difference that is clearly larger than its standard deviation as shown in Fig. 10. Panel (c) shows that the left and right values are close (indicating a consistency in production quality); however, the noise is actually less for the reverse direction.

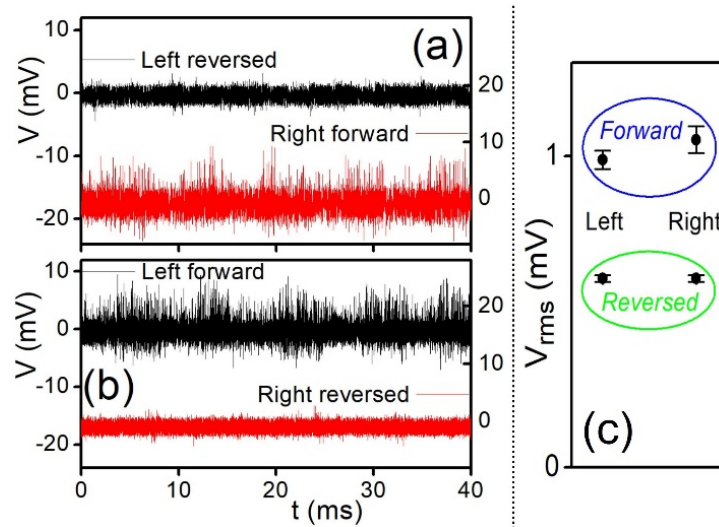


Fig. 10: Noise waveforms in interconnect M show a strong directional dependence in noise (panels (a) and (b)). Their rms noise voltages were calculated over the 200,000 samples of each oscilloscope trace and this process was repeated for multiple traces to obtain the means and standard deviations shown in panel (c).

Interconnect M also shows a directional dependence in its reflection sequence (see discussion in an earlier section) as shown in Fig. 11. The reverse-direction oscillations survive into the $\sim 1 \mu\text{s}$ time frame. Thus the optimum signal direction—which may depend on a system’s grounding scheme rather than the marked arrows—can be ascertained by the present measurements.

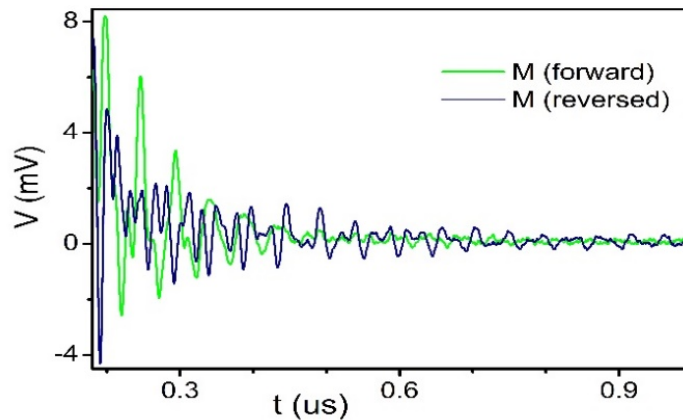


Fig. 11: Reflection sequence shows directional dependence in interconnect M.

Besides the noise waveforms, noise spectra were measured with the source end of each cable connected to a floating fully shielded 100Ω “shorting plug” following the setup of [1]. This emulates the star-ground configuration used by some audio systems in which one central component (e.g., the preamplifier or power amplifier) is externally grounded and other components are floated to avoid ground loops. The other end of the interconnect was connected to the DSO set to $1 \text{ M}\Omega$ DC-coupled input, no BWL, 5 MHz sampling rate, and 500 MHz analog bandwidth. The FFT (Fast Fourier Transform) was internally calculated and averaged for 545 sweeps within the oscilloscope.

The results are shown in Fig. 12. The cables are markedly different in their radio frequency interference (RFI) pickup. RF noise can undergo rectification-demodulation upon entering an amplifier and may contribute an audible signature to the music playback. The rms noise voltages were calculated in 3 ways, which are (for interconnects S, M, and G respectively): 27 μV , 2.6 mV, and 0.49 mV (unweighted over the entire 0–2.5 MHz bandwidth); 11.2 μV , 16.7 μV , and 18.6 μV (unweighted 0 Hz–22 kHz audible band); and 25.3 μV , 40.6 μV , and 44.5 μV (ITUR-468 weighted audible band [29–30]). The full-bandwidth noise of interconnects M and G is objectionably high, being only 24 and 38 dB below the 40.2 mV rms signal level used in the listening tests of [1]. If RF noise is mostly rejected by the input of the load component, the most relevant values would then be the ITUR-468 weighted ones whose electrical-power values for the 3 cables bear the ratios 1:2.57:3.08; and correspond to 64, 60, and 59 dB below the signal level used in [1].

[1] found an ITUR-468 ratio of 1:2.67 between their cables A (balanced) and B (unbalanced), which is almost identical to the present work’s ratio of 1:2.57 between S (unbalanced version similar to their cable A) and M (same as their cable B). It thus seems that a cable’s intrinsic shielding may be more relevant for reducing noise pickup than a balanced topology. Furthermore, balancing mainly helps with noise; it provides no benefit against the various TD signal alterations and NIC behaviors discussed in this work.

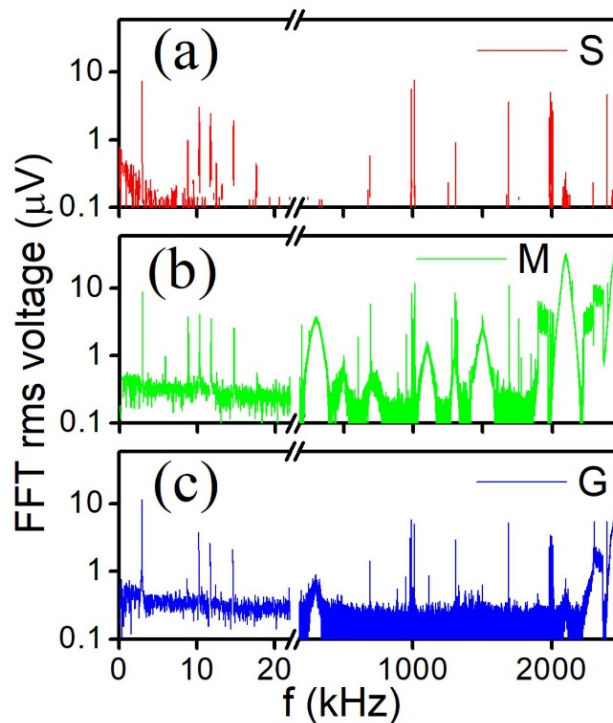


Fig. 12: Noise spectra of interconnects S, M, and G up to 2.5 MHz. The 0–22 kHz “audio band” is shown on a magnified horizontal scale before the axis break. The rms voltage (y axis) is the square root of the amplitude of each frequency component in the Fourier series.

V. Summary and Conclusions

The effect of cables on the sonic performance of an audio system has been a contentious subject for a few decades [31]. The controversy is fueled in part by the paucity of journal-published blind listening tests that prove there is at all an audible difference. Listening tests are tricky and can easily produce both false negative and false positive results; the relevant psychology and neurology is reviewed in [1, 32–36]. Another reason for disbelief in interconnect audibility may be due to a misguided focus on irrelevant measurements such as frequency response, resistance, and nominal reactance, whose resulting signal errors are indeed far below the presumed audibility thresholds.

The present work investigated other kinds of signal alterations during transmission through a cable, besides the above parameters. It was found that noise in some cables exists at audible levels. While the nominal reactive time constants may possibly be too short (<100 ns) for discernibility, the decay times arising from non-ideal effects are not obviously negligible (~1 μs), especially when multiple occurrences combine along the audio chain. Within the audio community at large, there tends to be a misunderstanding and underestimation of the

spectacular capabilities and extraordinary sensitivity of human hearing: For example, the ear can detect a cochlear basilar-membrane amplitude of ~ 1 pm [37–39] and has a temporal resolution in the microseconds that has no direct connection with the maximum audible frequency^k. [1 pm (picometer) is ~ 100 times smaller than an H atom]

The present work found clear systematic differences in the electrical performance of interconnect cables of different grades. Besides the electrical signal alterations studied here, vibrational effects (“microphonics”) may also potentially affect cable performance [17]. However unlike loudspeaker cables, interconnects lie in high impedance circuits and carry low currents. Thus they have smaller magnetic forces and induced voltages from mechanical motion. Another potential source of signal degradation in cables is triboelectric noise from internal motion; but it is estimated to be 180 dB below typical signal levels [45].

Previous work [1] demonstrated the audibility of cable pathways, pointing to differences in RF noise pickup as the likely cause. But it left open the question of whether the noise differences were due to shielding or balanced versus unbalanced topologies. The present work sheds light on that question by showing that its unbalanced cable S (of the same brand as cable A in [1]) is almost equally quiet. Furthermore, there are clear time-domain performance differences between the various interconnects tested. While cable manufacturers undoubtedly make a variety of measurements on their own products during the course of their development, the present results are of value to the consumer because they provide measurements across different brands made by a non-commercial entity.

References

- [1]. M. N. Kunchur, “Cable Pathways Between Audio Components Can Affect Perceived Sound Quality,” *J. Audio Eng. Soc.*, vol. 69, no. 6, pp. 398–409, (2021 June). DOI: <https://doi.org/10.17743/jaes.2021.0012> Download: <http://boson.physics.sc.edu/~kunchur/>
- [2]. H. R. E. van Maanen, “Temporal Decay: A Useful Tool for the Characterization of Resolution of Audio Systems?” presented at the 94th Convention of the Audio Engineering Society (1993 Mar.), paper 3480.
- [3]. H. R. E. van Maanen, “Requirements for Loudspeakers and Headphones in the ‘High Resolution Audio’ Era,” in *Proceedings of the 51st International Conference: Loudspeakers and Headphones (2013 Aug.)*, paper 1-3.
- [4]. H. R. E. van Maanen, “Is Feedback the Miracle Cure for High-End Audio?” (2017 May). <https://www.temporalcoherence.nl/cms/images/docs/FeedbackHvM.pdf>.
- [5]. W. Woszczyk, “Physical and Perceptual considerations for High-Resolution Audio,” presented at the 115th Convention of the Audio Engineering Society (2003 Oct.), paper 5931.
- [6]. N. Thiele, “Phase Considerations in Loudspeaker Systems,” presented at the 110th Convention of the Audio Engineering Society (2001 May), paper 5307.
- [7]. J. R. Stuart, “Coding for High-Resolution Audio Systems,” *J. Audio Eng. Soc.*, vol. 52, no. 3, pp. 117–144 (2004 Mar.).
- [8]. J. R. Stuart and P. Craven, “A Hierarchical Approach to Archiving and Distribution,” presented at the 137th Convention of the Audio Engineering Society (2014 Oct.), paper 9178.
- [9]. H. M. Jackson, M. D. Capp, and J. R. Stuart, “The Audibility of Typical Digital Audio Filters in a High-Fidelity Playback System,” presented at the 137th Convention of the Audio Engineering Society (2014 Oct.), paper 9174.
- [10]. J. D. Reiss, “A Meta-Analysis of High Resolution Audio Perceptual Evaluation,” *J. Audio Eng. Soc.*, vol. 64, no. 6, pp. 364–379 (2016 Jun.). <http://dx.doi.org/10.17743/jaes.2016.0015>.
- [11]. M. N. Kunchur, “Audibility of Temporal Smearing and Time Misalignment of Acoustic Signals,” *Electr. J. Tech. Acoust.*, vol. 17, pp. 1–18 (2007 Aug.). <http://www.ejta.org/en/kunchur1>.
- [12]. M. N. Kunchur, “Temporal Resolution of Hearing Probed by Bandwidth Restriction,” *Acta Acust. United Acust.*, vol. 94, no. 4, pp. 594–603 (2008 Jul./Aug.). <http://dx.doi.org/10.3813/AAA.918069>.
- [13]. M. van der Veen and H. R. E. van Maanen, “Non-linear distortions in capacitors”, presented at the 124th Convention of the Audio Engineering Society (2008 May).
- [14]. A. Yoneya, “Physical Characteristics of Analog Audio Cables and Their Effect on Sound Quality,” presented at the 148th Convention of the Audio Engineering Society (2020 May), paper 10338. <http://www.aes.org/e-lib/browse.cfm?elib=20755>.
- [15]. Y. Wang, “Frequency dependence of capacitance standards”, *Rev. Sci. Instrum.* vol. 74, no. 9, 4212-4215 (2003 Sept.); <https://doi.org/10.1063/1.1599063>
- [16]. A. Yoneya, “Perceptually Affecting Electrical Properties of Headphone Cable – Factor Hunting Approach,” presented at the 147th Convention of the Audio Engineering Society (2019 Oct.), paper 532. <http://www.aes.org/e-lib/browse.cfm?elib=20555>.
- [17]. R. Black, “Audio Cable Distortion Is Not a Myth!” presented at the 120th Convention of the Audio Engineering Society (2006 May), paper 6858. <http://www.aes.org/e-lib/browse.cfm?elib=13662>.
- [18]. J. D. Jackson, *Classical Electrodynamics*, 2nd ed. (John Wiley & Sons, Inc., New York, NY, U.S.A., 1975). ISBN-13: 978-0471431329; ISBN-10: 047143132X

^k In the literature an auditory temporal resolution of $\tau_{\text{ear}} \sim 8 \mu\text{s}$ is sometimes assumed, perhaps based on the ear’s canonical high-frequency limit of $f_{\text{ear}} \sim 20$ kHz and taking $\tau_{\text{ear}} = 1/2\pi f_{\text{ear}} = 8 \mu\text{s}$ (in analogy with a linear first-order low-pass filter). However, neural synchronous AND gating [11, 40–43] and aural non-linear mixing [12] in the auditory pathways negate the simple $\tau_{\text{ear}} = 1/2\pi f_{\text{ear}}$ relationship. [11] estimated $\tau_{\text{ear}} \sim 2 \mu\text{s}$ for a single ear for SSC (short-segment comparison) listening. Thus $\tau_{\text{ear}} \sim 1 \mu\text{s}$ is plausible for the more sensitive EMP (extended [duration] multiple-pass) listening protocol [1, 33–36] and the greater sensitivity through both ears [44]. SSC psychoacoustic measurements [11–12] have in fact established a τ_{ear} upper bound of $\sim 5 \mu\text{s}$.

- [19]. K. R. Fause, "Fundamentals of Grounding, Shielding, and Interconnection," *J. Audio Eng. Soc.*, vol. 43, no. 6, pp. 498–516 (1995 Jun.).
- [20]. S. R. Macatee, "Considerations in Grounding and Shielding Audio Devices," *J. Audio Eng. Soc.*, vol. 43, no. 6, pp. 472–483 (1995 Jun.).
- [21]. N. Muncy, "Noise Susceptibility in Analog and Digital Signal Processing Systems," *J. Audio Eng. Soc.*, vol. 43, no. 6, pp. 435–453 (1995 Jun.).
- [22]. B. Whitlock, "Balanced Lines in Audio Systems: Fact, Fiction, and Transformers," *J. Audio Eng. Soc.*, vol. 43, no. 6, pp. 454–464 (1995 Jun.).
- [23]. M. N. Kunchur, "Temporal aspects of musical sounds and their reproduction", article in preparation (please contact author for publication information).
- [24]. W. M. Hartmann, "On the perceptual segregation of steady-state tones", report 84 at the ATR Workshop on A biological framework for speech perception and production, Kyoto, Japan (1994).
- [25]. W. M. Hartmann, "Auditory grouping and the auditory periphery", *Proceedings of the First International Conference on Music Perception and Cognition*, pp. 299–304, Kyoto, Japan (1989).
- [26]. A. S. Bregman and J. Campbell, "Primary auditory stream segregation and the perception of order in rapid sequences of tones", *J. Exp. Psych.* vol. 89, 244–249 (1971).
- [27]. M. N. Kunchur, "3D Imaging in Two-Channel Stereo Sound: Portrayal of Elevation," *Appl. Acoust.*, vol. 175, 107811 (2021 Apr.). <https://doi.org/10.1016/j.apacoust.2020.107811>.
- [28]. J. Blauert, "Spatial Hearing: The Psychophysics of Human Sound Localization", revised edition (The MIT Press, Cambridge, MA, U.S.A., 1997).
- [29]. Audio Engineering Society, "Pro Audio Reference (W)," https://www.aes.org/par/w/#ITU_R_468.
- [30]. ITU-R, "Measurement of Audio-Frequency Noise Voltage Level in Sound Broadcasting," Recommendation ITU-R BS.468-4, https://www.itu.int/dms_pubrec/itu-r/rec/bs/R-REC-BS.468-4-198607-I!!PDF-E.pdf.
- [31]. D. Osher, "A Short History of High-End Cables", <https://www.theabsolutesound.com/articles/a-short-history-of-high-end-cables> (accessed Sept 18, 2021).
- [32]. T. Lund, A. M'akivirta, and S. Naghian, "Time for Slow Listening," *J. Audio Eng. Soc.*, vol. 67, no. 9, pp. 636–640 (2019 Sep.). <http://dx.doi.org/10.17743/jaes.2019.0023>.
- [33]. T. Lund and A. M'akivirta, "On Human Perceptual Bandwidth and Slow Listening," in *Proceedings of the AES International Conference on Spatial Reproduction - Aesthetics and Science* (2018 Jul.), paper P6-2. <http://www.aes.org/e-lib/browse.cfm?elib=19621>.
- [34]. M. A. Cohen, P. Cavanagh, M. M. Chun, and K. Nakayama, "The Attentional Requirements of Consciousness," *Trends Cogn. Sci.*, vol. 16, no. 8, pp. 411–417 (2012 Aug.). <http://dx.doi.org/10.1016/j.tics.2012.06.013>.
- [35]. M. A. Cohen, D. C. Dennett, and N. Kanwisher, "What is the Bandwidth of Perceptual Experience?" *Trends Cogn. Sci.*, vol. 20, no. 5, pp. 324–335 (2016 May). <http://dx.doi.org/10.1016/j.tics.2016.03.006>.
- [36]. D. Whitney, J. Haberman, and T. D. Sweeny, "From Textures to Crowds: Multiple Levels of Summary Statistical Perception," in J. S. Werner and L. M. Chalupa (Eds.), *The New Visual Neurosciences*, pp. 695–710 (MIT Press, Cambridge, MA, 2014).
- [37]. M. Lawrence, "Dynamic Range of the Cochlear Transducer," *Cold Spring Harb. Symp. Quant. Biol.*, vol. 30, pp. 159–167 (1965).
- [38]. B. M. Johnstone, K. J. Taylor, and A. J. Boyle, "Mechanics of the Guinea Pig Cochlea," *J. Acoust. Soc. Am.*, vol. 47, no. 2B, pp. 504–509 (1970).
- [39]. W. S. Rhode, "Observations of the Vibration of the Basilar Membrane in Squirrel Monkeys Using the Mossbauer Technique," *J. Acoust. Soc. Am.*, vol. 49, no. 4B, pp. 1218–1231 (1971).
- [40]. D. Oertel, R. Bal, S. M. Gardner, P. H. Smith, and P.X. Joris, "Detection of synchrony in the activity of auditory nerve fibers by octopus cells of the mammalian cochlear nucleus", *Proc. Nat. Acad. Sci.* 97, 11773–11779 (2000).
- [41]. N. L. Golding, D. Robertson, D. Oertel, "Recordings from slices indicate that octopus cells of the cochlear nucleus detect coincident firing of auditory nerve fibers with temporal precision", *J. Neurosci.* 15, 3138–3153 (1995).
- [42]. M. J. Ferragamo and D. Oertel, "Shaping of synaptic responses and action potentials in octopus cells", *Assoc. Res. Otolaryngol.* 21, 96 (1998).
- [43]. D. H. Johnson, "The response of single auditory-nerve fibers in the cat to single tones: synchrony and average discharge rate", Ph.D. thesis, Department of Electrical Engineering, MIT, Cambridge, MA (1974).
- [44]. B. C. J. Moore, "Introduction to the Psychology of Hearing", 5th ed. (Academic Press, San Diego, CA, U.S.A., 2003). ISBN 0-12-505628-1.
- [45]. I. Sinclair, "Audio and Hi-Fi Handbook", Newnes publishing, Third Edition (1998). ISBN-10: 075063636X, ISBN-13: 978-0750636360.